Magneto-optical features of Ni-substituted $CoFe_2O_4$ nano spinel ferrites and its photocatalytic activity

P. Kalaivani[1], G. Mathubala[2*]

[1]Research Scholar, Department of Chemistry, Bharath Institute of Higher Education and Research, BIST, Chennai -73, Tamil Nadu, India, Email: mathubala.che@bharathuniv.ac.in
[2]Professor, Department of Chemistry, Bharath Institute of Higher Education and Research, BIST, Chennai - 73, Tamil Nadu, India, Email: madhu2705@gmail.com
*Corresponding Author

Received: 10.07.2024 Revised: 14.08.2024 Accepted: 22.09.2024

ABSTRACT
Ni-substituted cobalt ferrite ($Co_{1-x}Ni_xFe_2O_4$, x = 0.0 to 1.0) nano spinel ferrites (NSFs) with different particle sizes were created using the microwave combustion process with urea fuel. Powder XRD diffraction was used to characterize the acquired spinel ferrites, and HR-SEM and HR-TEM were used to examine the average size and grain shape. Nitrogen adsorption and desorption isotherms are used to estimate the BET-specific surface area, pore size distribution, and pore volume of $Co_{1-x}Ni_xFe_2O_4$ nanomaterials. The room temperature magnetization of $Co_{1-x}Ni_xFe_2O_4$ NSFs with various Ni contents (x = 0.2, 0.4, 0.6, 0.8, and 1.0) was measured using VSM (vibrating sample magnetometer). To estimate the catalytic activity of $Co_{1-x}Ni_xFe_2O_4$ NSFs, the degradation of 4-NP has been studied with $NaBH_4$ at room temperature. Moreover, reduction reactions are achieved with 2 $\times 10^{-5}$ M of sodium borohydride ($NaBH_4$) and $Co_{1-x}Ni_xFe_2O_4$ with NSF catalysts. $CoFe_2O_4$ shows zero activity in the reduction reaction. Surprisingly, it has been perceived that the catalytic efficiency is improved with the introduction of Ni content with $CoFe_2O_4$ lattice. Among all compositions, $Co_{0.8}Ni_{0.2}Fe_2O_4$ shows a maximum rate constant. Different mechanisms are investigated using the acquired results, and their relevance to magnetism and structure is explained.

Keywords: microwave combustion, nano spinel ferrites, $CoFe_2O_4$, catalytic activity

1. INTRODUCTION

Nanoparticles of ferrites with large coercivity and saturation magnetization are generally used in making recording devices, permanent magnets, electric motors, automotive power, etc. The coercivity and saturation magnetization properties are improved by varying chemical composition and micro-structural characteristics. Ferrite nanoparticles are also applied in chemical reactions due to their catalytic, photocatalytic, and photoelectrochemical properties [1-2].

Generally, cobalt ferrites can be easily separated after the reaction; reusability is also magnetic; and catalytic recyclability makes it more attractive among young researchers. Furthermore, a unique mixture of large coercivity with moderate magnetized properties supports it as an effective hard magnetic material. These can generate $CoFe_2O_4$ nanoparticles seemingly for magnetic recording applications like auditory and audiovisual tape and high-density numerical recording disks [3-5].

Cobalt ferrite and nickel ferrite have high and low magneto-crystalline anisotropy constants, respectively [6-8]. Hence, a suitable mixing of these two Centro symmetric magnetic materials can produce exciting and innovative magnetic properties. However, complexity may arise in $Co_{1-x}Ni_xFe_2O_4$ materials due to differences in magneto-crystalline anisotropy constants.

More materials with a zero value of anisotropy constant can be produced by cooperating these ferrites in a suitable proportion, and this can generate intrinsic properties in the final materials [9].

Biologically, chemically stable toxic dyes and nitroaromatic compounds are difficult to remove in wastewater from dye and pigment industrial sectors by natural degradation processes [10-15]. Moreover, derivatives of phenol show a vital role in water pollutants based on stability in water. Nitrogen-containing phenols are mostly concerned with the cause of severe health issues and significant poisons for catalysts [16]. Due to their significant water solubility, these phenol derivatives are found in surface waters, groundwater wells, etc. Hence, the successful elimination of hazardous impurities and before discharge transformation in too few useful products is of greatest importance to achieve quality drinking water.

Thus, the treatment of impurities with 4-nitrophenol is a little inevitable. Some other treatment modes of techniques, like photocatalytic degradation [17-18], ozonation [19], peroxide oxidation [20], the Fenton process [21], and the electrochemical method [22-23] are generally preferred for degradation methods. But ferrites can be used as a catalyst for the degradation methods, which is an inexpensive and facile method but not practical. Feng et al. achieved more than 95% conversion by using Cu ferrite nanoparticles as a catalyst for the reductant of 4-Nitro Phenol with $NaBH_4$ as a reducing agent. Sodium borohydride is a weak reducing agent, which can be achieved in a liquid medium also. The catalytic efficiency of MFe_2O_4 nano ferrites was estimated for the reductant of Nitro Phenol with $NaBH_4$ as a reducing agent [24-27]. From the above reference, it was found that 50 equivalents of $NaBH_4$ are the optimum amount for catalytic efficiency.

In this study, $Co_{1-x}Ni_xFe_2O_4$ NSFs were synthesized from metal nitrates, and urea with deionized water with microwave via the solution combustion method followed by crushing. The first part of the work discussed the textural and morphological characteristics of $Co_{1-x}Ni_xFe_2O_4$ nanoparticles and other analysis to verify the size, position, and distribution of the particles. The second part deals with the degradation kinetics of 4-nitrophenol in aqueous $Co_{1-x}Ni_xFe_2O_4$ NSF suspensions with sodium borohydride as the reductant.

2. Material Synthesis

2.1. Synthesis of $Co_{1-x}Ni_xFe_2O_4$ ($0.0 \le x \le 1.0$) NSFs

The spinel $Co_{1-x}Ni_xFe_2O_4$ was synthesized from the chemicals (Merck) received without purification. The fuels used for the reaction to synthesize the compound are nickel nitrate (98%), ferric nitrate (98%), cobalt nitrate (98%), and urea. Nickel with different molar ratios ($Co_{1-x}Ni_xFe_2O_4$ with x=0.0, 0.2, 0.4, 0.6, 0.8, and 1.0) is added to $CoFe_2O_4$ NSFs to get different compositions. The un-doped cobalt ferrite was prepared by the method of microwave. The originator's mixture with urea was kept in an ordinary oven and exposed to an energy of 2.45 GHz at 750 W for 10 min. Because urea has a high dielectric loss in microwave heating systems, the reaction will proceed quickly. As a result, a solid powder was obtained. This obtained powder was cleaned thoroughly with ethanol and dried at the temperature of 70 ^{o} C for 1 hour. After 1 hour, the powdered samples were labelled as $CoFe_2O_4$, $Co_{0.8}Ni_{0.2}Fe_2O_4$, $Co_{0.6}Ni_{0.4}Fe_2O_4$, $Co_{0.4}Ni_{0.6}Fe_2O_4$, $Co_{0.2}Ni_{0.8}Fe_2O_4$, and $NiFe_2O_4$ NSFs.

3. RESULTS AND DISCUSSION

3.1. Nano-spinel ferrite: Preparation

$Co_{1-x}Ni_xFe_2O_4$ NSFs were synthesized from an aqueous solution with metal nitrates, urea, and deionized water using a microwave via the solution combustion method followed by crushing. The combustion method has more advantages as it does not need any more chemicals because of its low budget, lack of by-product formation, and being environmentally friendly. In a microwave oven, microwave energy is absorbed by dealings of microwave radiation with the material and converted to thermal energy uniformly throughout a reaction container. The microwave combustion method has been rapidly developed as the energy of microwaves reacts with the molecular level of reactants. Thus, by rapid heating of materials, faster kinetics with better reproducibility of the products were observed. To estimate the catalytic action of the produced materials, the degradation of 4-Nitro Phenol has been preferred as the representative member of the pollutant group because of its environmental importance.

3.2. Microstructure analysis

The structural aspects of prepared spinel $Co_{1-x}Ni_xFe_2O_4$ (x = 0.2, 0.4, 0.6, 0.8, and 1.0) NSF catalysts have been explored by powder-XRD measurements. XRD experiments are carried out to know the crystallographic structure and the size of the particle. The structure and size of the crystallite of NSFs can also be verified by powder X-ray diffraction patterns. Figure 1 displays the X-ray diffraction pattern $Co_{1-x}Ni_xFe_2O_4$ (x = 0.2, 0.4, 0.6, 0.8, and 1.0) NSFs. The powder XRD diffraction peaks (2θ) appear at 29.38, 34.84, 36.11, 42.83, 52.95, 55.73, and 62.83 related to (220), (311), (222), (400), (422), (511), (440) planes, respectively. It reveals that prepared materials exhibit the diffraction reflections of the spinel phase and show the uniqueness of a single-phase cubic spinel structure, which are matched well with JCPDS Card No. 22-1086 for $CoFe_2O_4$ and JCPDS Card No. 10-0325 for $NiFe_2O_4$, respectively [26]. The discovered peaks correspond to the $Co_{1-x}Ni_xFe_2O_4$ structure. The absence of other peaks assures that there are no impurity phases and shows good substitution of dopant in ferrite matrices. The sharp and high-intensity diffraction peaks can prove the pure crystallinity of the prepared materials.

The average crystallite size has been evaluated using Debye Scherer's formula, estimated from the most intense peak (311). However, the particle size calculated by this technique cannot separate the contribution from individual oxide phases over the full-width half maximum of the diffraction maxima.

The values are displayed in Table 1. The data includes the particle size of the samples, which is purely based on Ni percentage. This is lower (15.2 nm) for undoped $CoFe_2O_4$ and is increased to 16.8 nm for $Co_{0.8}Ni_{0.2}Fe_2O_4$ to 21.2 nm for $Co_{0.2}Ni_{0.8}Fe_2O_4$. The increase in size (crystallite) is based on the variation in Ni^{2+} ion and Co^{2+} ion concentration of the ferrite composite. The increase in particle size is owing to the much larger ionic radius of Ni^{2+} ions than that of Co^{2+} ions. Further, the average combustion temperature may also influence the crystallinity and crystallite size, which have been ignored here, as similar; the preparation method has been followed to synthesize all the materials.

Further, compared to $CoFe_2O_4$, a small shift to the lower diffraction angle associated with $Co_{1-x}Ni_xFe_2O_4$ materials in the X-ray diffractogram reveals an overall expansion of the lattice with the increase in Ni concentration. Indeed, there is a small change in the lattice parameters, and it depends on the amount of Ni doping. To understand the shift in peak, Rietveld analysis has been carried out for all the materials. Rietveld refinement analyses are done to find the structural features of the samples using the XPERT PLUS program. From Figures 2a and 2b, it is clear that the observed XRD patterns of the synthesized materials ($Co_{0.6}Ni_{0.4}Fe_2O_4$, $Co_{0.8}Ni_{0.2}Fe_2O_4$) are well agreed with computed patterns without any additional phases. Figure 3 displays a deep curve that completely matches the calculated and observed patterns. The refining confirmed the sample's spinel structure. Rietveld analysis also clearly suggests that the increase in the lattice parameters.

All composition's computed lattice parameters correspond well with the findings obtained using the Rietveld refinement method, as displayed in Table 1 and Figure 3a. From Table 1, it is noticed that the lattice parameters of $CoFe_2O_4$ NSFs are 8.378 Å and are increased to 8.421 Å for the $NiFe_2O_4$ NSF. mainly occurs by the difference in ionic radius of Co^{2+} ion (0.7 Å) and Ni^{2+} ion (0.73 Å) cations. Figure 3b depicts the change in crystallite size with the incorporation of Ni substituted into $CoFe_2O_4$. The graph shows that the particle size increases as the number of dopants increases (Figures 1 and 3a), which further confirms the effective substitution of Ni^{2+} in the lattice by Co^{2+}ions.

3.3. HR-SEM analysis

The morphology and the textural properties of prepared materials are explored using HR-SEM. Figures 4(a-d) show the HR-SEM images of (a) $Co_{0.8}Ni_{0.2}Fe_2O_4$, (b) $Co_{0.6}Ni_{0.4}Fe_2O_4$, (c) $Co_{0.4}Ni_{0.6}Fe_2O_4$, and (d) $Co_{0.2}Ni_{0.8}Fe_2O_4$ NSFs, respectively. HR-SEM images reveal that the sample contains sphere-like nanoparticles (irregularly shaped) that agglomerate. Moreover, the agglomeration and combination of the particles are attributed to the strong intermolecular friction of microwave irradiation converts microwave energy into internal heat energy. Further, it shows the pores of the sample are in the range of 40 - 60 nm. This porous nature of the sample supports the surface area analysis.

Furthermore, the particles are closely packed together and have diameters less than 100 nm. The microwave irradiation approach achieved such small particles of samples with great surface area in a few minutes due to microwave energy heating. The variance in particle size observed in HR-SEM images for all samples could be attributed to agglomeration effects generated by the magnetic nature of the materials at annealing temperature.

3.4. HR-TEM analysis

Figures 5(a-d) illustrate the HR-TEM images of (a) $Co_{0.8}Ni_{0.2}Fe_2O_4$, (b) $Co_{0.6}Ni_{0.4}Fe_2O_4$, (c) $Co_{0.4}Ni_{0.6}Fe_2O_4$, and (d) $Co_{0.2}Ni_{0.8}Fe_2O_4$, NSFs are composed of spherical nanoparticles that are consistent with HR-SEM pictures. In addition, the sample sizes may range from 30 to 50 nm. The size of the crystalline sample acquired from powder XRD analysis is closely related to the particle sizes measured by HR-TEM. Agglomeration of particles is also observed in HR-TEM images, which is attributed to the high-temperature synthesis process.

3.5. Magnetic investigation

The room temperature magnetization of $Co_{1-x}Ni_xFe_2O_4$ NSFs with several Ni compositions (x = 0.2, 0.4, 0.6, 0.8) is measured with a VSM, and the resulting M-H curves are shown in Figure 6. The measured magnetic data from the VSM in the value of ± Koe confirms the magnetic behavior of the sample.

The substitution of Ni content on $CoFe_2O_4$ spinel changes the M_s and M_r. VSM measurement; all the samples demonstrated soft and ferromagnetic properties of the produced materials. Chemical composition, cation distribution, and particle size in spinel ferrites' tetrahedral (A) and octahedral (B) sites all play important roles in determining the material's magnetic characteristics. The nonlinear and reversible characteristic of hysteresis loops of all samples indicates the soft nature of ferrite samples. The value of saturation magnetization (figure 6) is maximum for the composition of X = 0.2 and then decreases gradually with an increase in Ni dopant. When the Co2+ ion is replaced by the Ni2+ ion in the Co-Ni ferrite combination, the Ni2+ ions preferentially travel to the A site, while the Co2+ ions move to

the B site in a cubic spinel lattice. Therefore, diamagnetic compounds like Ni2+ dilute the concentration of Fe3+ ions at the A site. As a result, as the concentration of Ni dopant in ferrite materials increases, the saturation magnetization falls. The saturation magnetization values are shown in Table 2.

3.6. Photocatalytic activity of $Co_{1-x}Ni_xFe_2O_4$ NSFs

The catalytic activity of $Co_{1-x}Ni_xFe_2O_4$NSFsis was evaluated from the degradation of 4-nitrophenol which was analysed including $NaBH_4$ at room temperature. $NaBH_4$ is chosen as a reducing agent to reduce 4-nitrophenol to 4-aminophenol. Hence the reaction is selected as a representation reaction because it can be easily observed with UV-visible spectroscopy. In acidic environments, 4-Nitrophenol absorbs at 318 nm, whereas 4-AP absorbs at 300 nm; thus, degradation of 4-NP can be explored by a gradual decline in the nitrophenol peak and the presence of an aminophenol peak. The addition of NaBH4 to 4-nitrophenol causes the absorption peak to shift from 318 to 402 nm due to the production of phenolate ions. Figure 7 depicts the typical breakdown of 4-nitrophenol and the production of 4-aminophenol by Co-ferrite-based composites.

First, the degradation of 4-nitrophenol and production of 4-aminophenol are carried out in the presence of cobalt ferrite. In this attempt, we found that undoped $CoFe_2O_4$ is fully inactive as a catalyst in all conditions. Then the degradation reaction has been tried in the combination of Ni dopant nanoparticles as catalysts. Surprisingly, after doping with the Ni^{2+} ion, the catalytic efficiency is dramatically enhanced. So, we investigate different doping concentrations to degrade 4-NP and develop 4-AP.

The catalyst and sodium borohydride are both present and are identified to be necessary for the reductant reaction. Initially, optimization of the amount of $NaBH_4$ has been carried out. The amount of $NaBH_4$ is varied in the reaction medium from 2×10^{-6} to 2×10^{-5} M, and it was noticed that the reaction completion time decreases with a rise in the amount of reducing agent up to 2×10^{-5} M with a further increase of $NaBH_4$, causing very less improvement in the rate of catalytic reaction. So, 2×10^{-5} M of $NaBH_4$ is found to be the optimum amount for the degradation reaction in the present reaction condition. For further analysis, the rate constant of the reaction after 8 min of the reaction with varying $NaBH_4$ has been evaluated. Figure 8 shows the rate of reduction of 4-NP with varied concentrations of $NaBH_4$.

The optimization of Ni doping is analysed, and it is seen that as the number of catalysts increases, the reaction accelerates due to an increase in the number of accessible catalytic sites for the reduction reaction to occur. In a comparative investigation, the reduction reactions are performed in the presence of 2×10^{-5} M of $NaBH_4$ (the reducing agent) and varying amounts (100 mg to 300 mg) of different $Co_{1-x}Ni_xFe_2O_4$ NSFs as catalysts. It is observed that with an increase in the quantity of catalyst, there is an increase in the reduction rate of 4-NP. However, more catalyst makes it difficult to track the kinetic investigations by measuring absorbance changes. Hence, the optimum nanoparticle dosage is kept at 300 mg.

The inclusion of the catalyst is expected to trigger the degradation reactions. The strength of the absorption peak at 400 nm gradually decreases, revealing a new peak at 300 nm, indicating that 4-nitrophenol has been converted to 4-aminophenol. Figure 9 shows that 4-amino phenol absorbs at 300 nm in the UV-visible spectrum in the presence of sodium borohydride.

The reduction reactions are performed with 2×10^{-5} M of sodium borohydride ($NaBH_4$) and $Co_{1-x}Ni_xFe_2O_4$ (x = 0.0, 0.2, 0.4, 0.6, 0.8, and 1.0) NSFs as catalysts. $CoFe_2O_4$ NSFs show zero activity for the reduction reaction, whereas $NiFe_2O_4$ NSFs show activity for the degradation. Hence, ferrites synthesized with various compositions of Ni and Co have been investigated under the same reaction conditions. Surprisingly, it has been observed that the addition of Ni to the cobalt ferrite lattice significantly improves catalytic efficiency. After 10 minutes of the reaction, the 4-NP solution is completely degraded by 4-Amino Phenol. However, with the incorporation of more and more Ni-cobalt ferrite, the time of reduction increases but the same quantity of 4-AP is degraded.

This can be better understood from Figure 10. No decolorisation of 4-NP solution has been observed for some time of 100 min in the absence of the ferrite. As there is an excess concentration of $NaBH_4$, the reduction reaction may be considered to have pseudo-first-order kinetics. The rate law equation below could be used to derive pseudo-first-order rate constants.

$\ln (A_t/A_0) = -K_o t$

Where A_t and A_0 are the absorbances at time t with t = 0.

Figure 10 depicts the reduction of 4-nitrophenol with Co0.8Ni0.2Fe2O4 NSFs and 2 ×10-5 M of NaBH4. The plot displays ln (At/A0) vs. (t) for different compositions of Co1-xNixFe2O4 NSFs. Table 2 displays the estimated rate constant values based on the slope of the straight line generated from the plot of ln (At/A0) vs. time (t). Increasing the influence of the catalyst raises the reaction's rate constant. Rate constant values for $Co_{0.8}Ni_{0.2}Fe_2O_4$ and $Co_{0.2}Ni_{0.8}Fe_2O_4$ nanoparticles are found to be 4.4 and 0.9 min^{-1}, respectively. Hence, with the introduction of Ni-substituted $CoFe_2O_4$ NSFs, the degradation ability is also

optimum. $Co_{0.8}Ni_{0.2}Fe_2O_4$ NSFs show the maximum rate constant and suitable pore volumes of $Co_{0.8}Ni_{0.2}Fe_2O_4$ nanocatalyst, making it appropriate for 4-Nitro Phenol (4-NP) to degrade on the catalyst surface. Moreover, it can be stated that the lower concentration of nickel in the cobalt ferrite matrix is finely dispersed, and it is optimum to reap maximum benefit for the catalytic activity.
To examine the reusability, the catalyst from the reaction mixture is recovered through the centrifugation method. When the solution is centrifuged, all the present nanoparticles settle down into the centrifuge tube, and the aqueous solution left at the top should be transferred carefully. The process is repeated twice, and finely dispersed black particles are obtained. After that, it is washed with distilled water 3-4 times, and the catalytic reactions are performed with a reused catalyst (up to 5 cycles) under similar reaction conditions. The results of a catalytic experiment using the same catalyst under the same conditions indicate that the regenerated particles retain good activity even in the fifth cycle. In these investigations, the measured reaction rate with reused catalyst is comparable, indicating that the catalyst is recyclable and reusable with no substantial loss of activity.

CONCLUSIONS

A structure of Ni-substituted cobalt ferrite NSFs with the formulation $Co_{1-x}Ni_xFe_2O_4$ (x = 0.0, 0.2, 0.4, 0.6, 0.8, and 1.0) was synthesized via the microwave combustion method. The materials are characterized by XRD and electron microscopic techniques. X-ray diffraction and Rietveld's study confirm the development of spinel $Co_{1-x}Ni_xFe_2O_4$ NSFs with well-crystallised structures and no other secondary phase formation. The samples' mean crystallite diameters range from 15.2 to 22.5 nm, as determined using the Debye-Sherrer formula. Ni2+ ions have a larger ionic radius than Co2+ ions, leading to an increase in the lattice parameter from 8.378 Å to 8.421 when Ni concentration increases. The spherical morphology of the nanoparticles is confirmed by high-resolution scanning electron microscopy and high-resolution transmission electron microscopy images. VSM tests for all compositions demonstrate that the materials are ferromagnetic; the value of Ms for pure CoFe2O4 NSFs is 56.3 emu/g, and it drops from 56.3 to 22.2 emu/g as Ni concentration increases. This may be due to the diamagnetic nature of Ni^{2+} ions. The ferromagnetic behavior is confirmed by the M-H loops. The fine particle size of these spinel's is evidenced by the scanning electron micrographs. The enhanced catalytic activity of spinel $Co_{1-x}Ni_xFe_2O_4$ NSF catalysts is also explored. It can catalyze the degradation of 4-NP with sodium borohydride. CoFe2O4 NSFs have no activity in the reduction reaction, but when Ni is added to the cobalt ferrite lattice, the catalytic efficiency increases significantly. Among all compositions, $Co_{0.8}Ni_{0.2}Fe_2O_4$ NSF shows the maximum rate constant. Furthermore, it is consistently stable and demonstrates an affordable, environmentally friendly alternative catalyst that is better suited for wastewater treatment. This catalyst can be reused without losing considerable activity.

Conflict of Interest

There are no conflicts of interest.

REFERENCES

[1] Baykal, A., Karaoglu, E., Sozeri, H., Uysal, E., Toprak, M. S.: J. Supercond. Nov. Magn. 26, 165 (2013).
[2] Karaoglu, E., Baykal, A.: J. Supercond. Nov. Magn.27, 2041 (2014)
[3] Manikandan, A., Durka, M., Arul Antony, S.: J. Supercond. Nov. Magn. 27, 2841 (2014).
[4] Manikandan, A., Durka, M., Arul Antony, S.: J. Supercond. Nov. Magn. 28, 209 (2015)
[5] Zhongli, W., Xiaojuan, L., Minfeng, L., Ping, C., Yao, L., Jian, M.: J. Phys. Chem. B 112, 11292 (2008)
[6] Agrafiotis, C. C., Pagkoura, C., Zygogianni, A., Karagiannakis, G., Kostoglou, M., Konstandopoulos, G. A.: Int. J. Hydrogen Energy 37, 8964 (2012)
[7] Borgohain, C., Senapati, K. K., Sarma, K. C., Phukan, P.: J. Mol. Catal. A: Chem. 363, 495 (2012)
[8] Kumbhar, V. S., Jagadale, A. D., Shinde, N. M., Lokhande, C. D.: J. Appl. Surf. Sci. 259, 39 (2012)
[9] G. Mathubala, A. Manikandan, S.A. Antony, P. Ramar, Photocatalytic degradation of methylene blue dye and magneto-optical studies of magnetically recyclable spinel NixMn1-xFe2O4 (x= 0.0–1.0) nanoparticles, Journal of Molecular Structure 1113 (2016) 79-87.
[10] Koseoglu, Y., Baykal, A., Toprak, M. S., Gozuak, F., Basaran, A. C., Aktas¸ B.: J. AlloysCompd.462, 209 (2008)
[11] Ramankutty, C.G., Sugunan, S.: App. Catal. A: Gen. 218, 39 (2001)
[12] Kiselev, S. I., Sankey, J. C., Krivorotov, I. N., Emley, N. C., Schoelkopf, R. J., Buhrman, R. A., Ralph, D. C.: Nature 425, 380 (2003).
[13] Borgohain, C., Senapati, K. K., Sarma, K. C., Phukan, P.: J. Mol. Catal. A: Chem. 363-364 (2012) 495-500.
[14] Yan, K., Wu, X., An, X., Xie, X.: J. AlloysCompd.552, 405 (2013)

[15] Koseoglu, Y., Alan, F., Tan, M., Yilgin, R., Ozturk, M.: Ceram. Int. 38, 3625 (2012)
[16] Koseoglu, Y., Baykal, A., Gozuak, F., Kavas, H.: Polyhedron 28, 2887 (2009)
[17] Koseoglu, Y., Alan, F., Tan, M., Yilgin, R., Ozturk, M.: Ceram. Int. 38, 3625 (2012)
[18] Pillai, V., Shah, D. O.: J. Magn. Magn. Mater. 321, 2170 (2009)
[19] Cabuil, V., Dupuis, V., Talbot, D., Naveu, S.: J. Magn. Magn. Mater. 323, 1238 (2011)
[20] Cheng, F., Peng, Z., Liao, C., Xu, Z., Geo, S., Yan, C., Wang, D.: Solid State Commun. 107, 471 (1998)
[21] Sajjia, M., Oubaha, M., Hasanuzzaman, M., Olabi, A. G.: Ceram. Int. 40, 1147 (2014)
[22] Koseoglu, Y., Oleiwi, M. I. O., Yilgin, R., Kocbay, A. N.: Ceram. Int. 38, 6671 (2012)
[23] Arora, M., Chauhan, S., Sati, P. C., Kumar, M.: J. Supercond. Nov. Magn.27, 1867 (2014)
[24] Khan, M. A., Islam, M. U., Ishaque, M., Rahman, I. Z.: J. Alloys Compd. 519, 156 (2012)
[25] Baykal, A., Guner, S., Demir, A.: J. Alloys Compd. 619, 5 (2015)
[26] Kurmude, D. V., Kale, C. M., Aghav, P. S., Shengule, D. R., Jadhav, K. M.: J. Supercond. Nov. Magn.27, 1889 (2014)
[27] Kumar, L., Kumar, P., Srivastava, S. K., Kar, M.: J. Supercond. Nov. Magn.27, 1677 (2014)
[28] G. Mathubala, A. Manikandan, S. Arul Antony, P. Ramar, Enhanced photocatalytic activity of spinel Cu x Mn1–x Fe2O4 nanocatalysts for the degradation of methylene blue dye and opto magnetic properties, Nanoscience and Nanotechnology Letters 8(5) (2016) 375-381.

Table 1. XRD parameter and textural properties of $Co_{1-x}Ni_xFe_2O_4$ NSFs

x	Sample	D_{XRD} (nm)	a (Å)
0.0	$CoFe_2O_4$	22.5	8.421
0.2	$Co_{0.8}Ni_{0.2}Fe_2O_4$	21.2	8.415
0.4	$Co_{0.6}Ni_{0.4}Fe_2O_4$	19.6	8.405
0.6	$Co_{0.4}Ni_{0.6}Fe_2O_4$	17.9	8.391
0.8	$Co_{0.2}Ni_{0.8}Fe_2O_4$	16.8	8.383
1.0	$NiFe_2O_4$	15.2	8.378

Table 2. Ms of $Co_{1-x}Ni_xFe_2O_4$ NSFs and Rate constant values calculated from the slope of the straight line obtained from the plot of ln (A_t/A_0) vs. time (t) for different $Co_{1-x}Ni_xFe_2O_4$ NSFs

Sample	Ms (emu/g)	Rate constant x 10 (min^{-1})
$CoFe_2O_4$	56.3	2.97
$Co_{0.8}Ni_{0.2}Fe_2O_4$	53.8	4.4
$Co_{0.6}Ni_{0.4}Fe_2O_4$	41.6	2.0
$Co_{0.4}Ni_{0.6}Fe_2O_4$	31.3	1.2
$Co_{0.2}Ni_{0.8}Fe_2O_4$	22.2	0.9
$NiFe_2O_4$	10.7	0.0

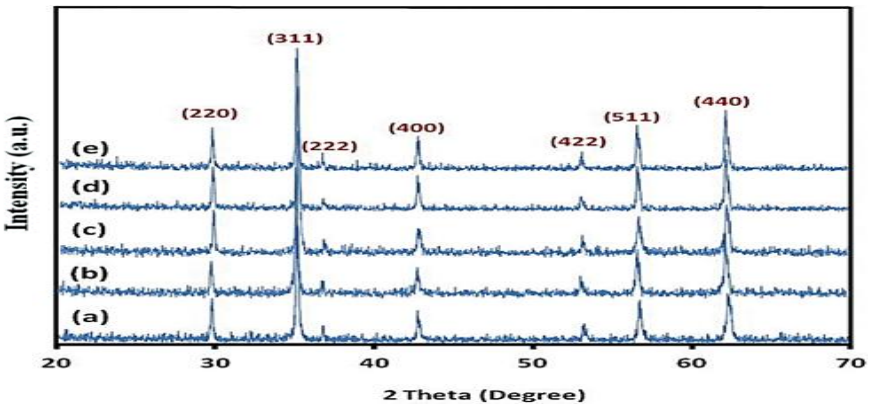

Figure 1
Figure 1(a-e).

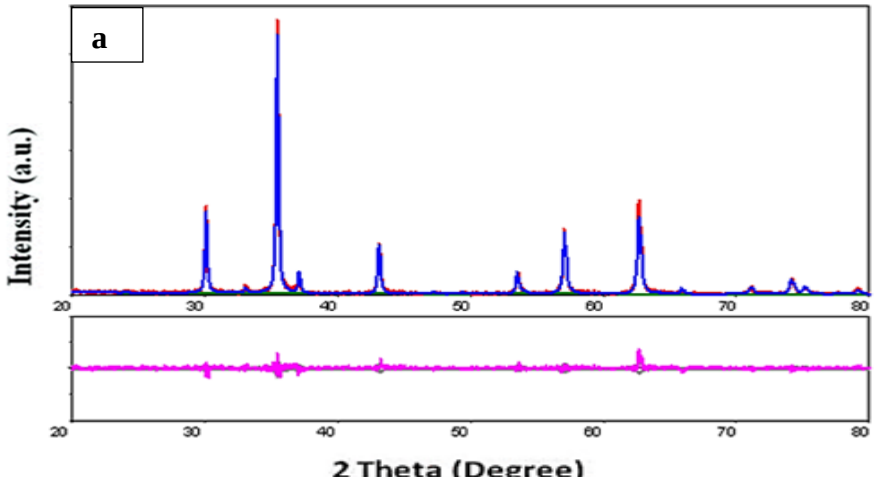
a
Intensity (a.u.)
20
30
40
50
60
70
80
2 Theta (Degree)

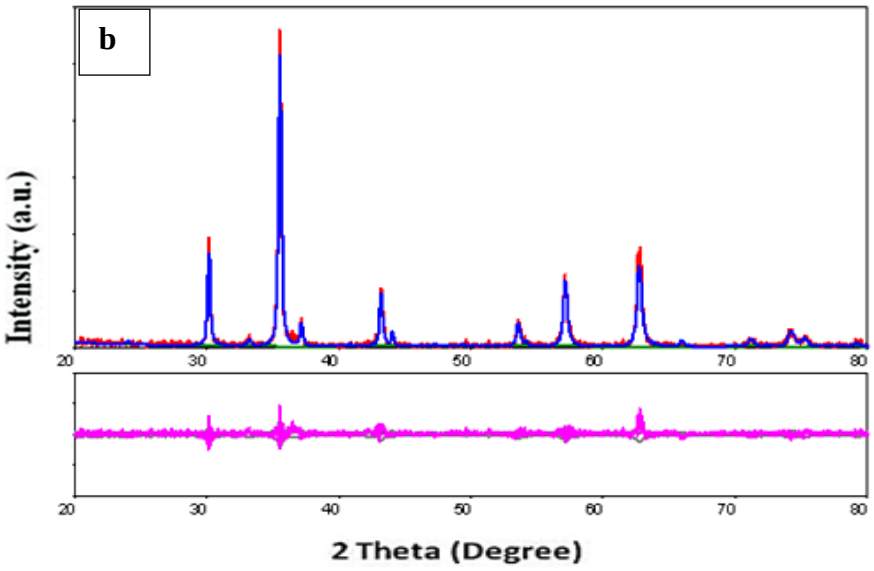
b
Intensity (a.u.)
20
30
40
50
60
70
80
2 Theta (Degree)

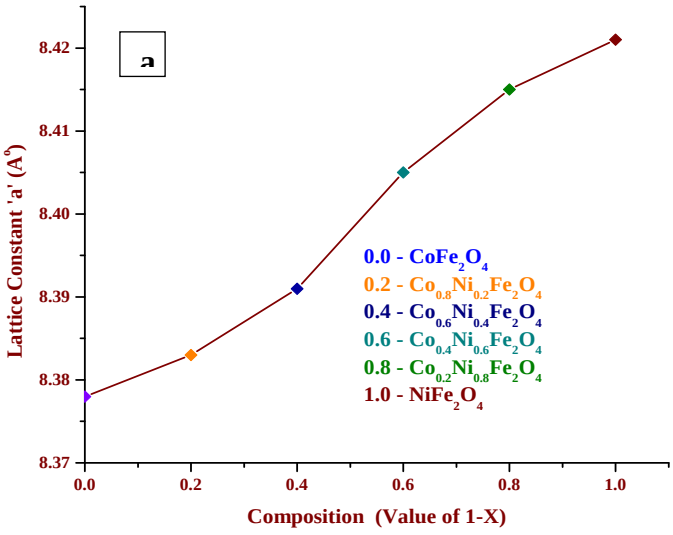
a
Lattice Constant 'a' (A°)
8.37
8.38
8.39
8.40
8.41
8.42
0.0
0.2
0.4
0.6
0.8
1.0
Composition (Value of 1-X)
0.0 - CoFe2O4
0.2 - Co0.8Ni0.2Fe2O4
0.4 - Co0.6Ni0.4Fe2O4
0.6 - Co0.4Ni0.6Fe2O4
0.8 - Co0.2Ni0.8Fe2O4
1.0 - NiFe2O4

\

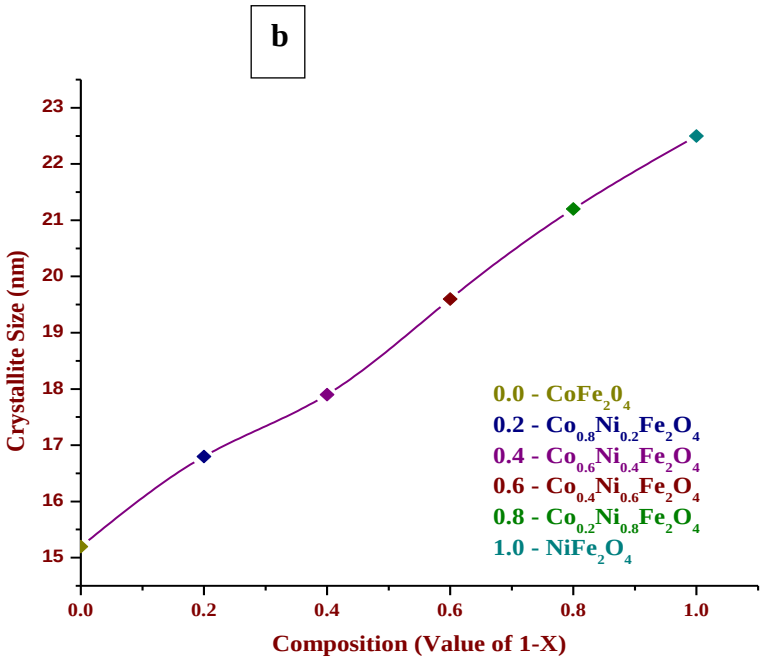

Figure 3(a-b).

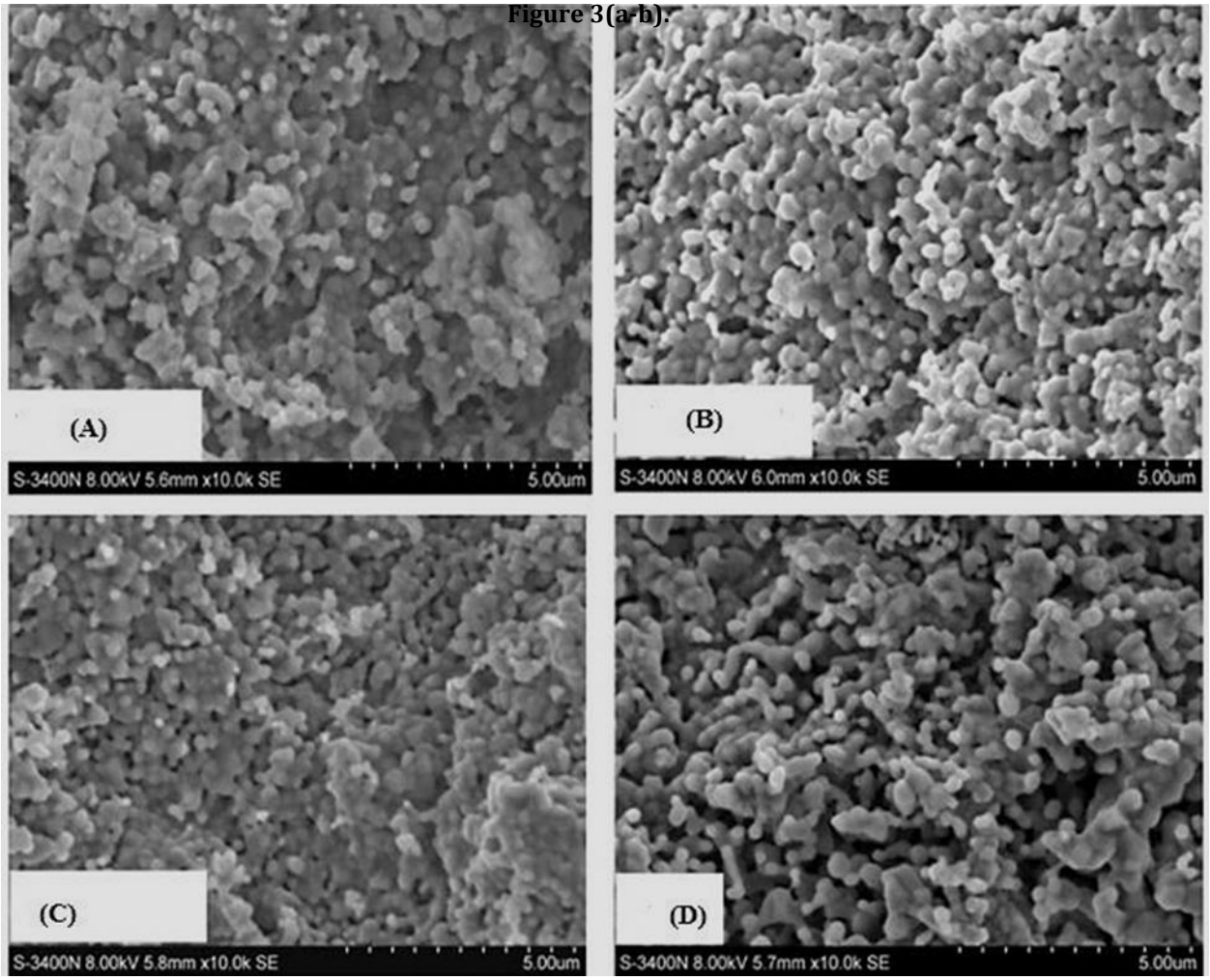

Figure 4 (A-D).

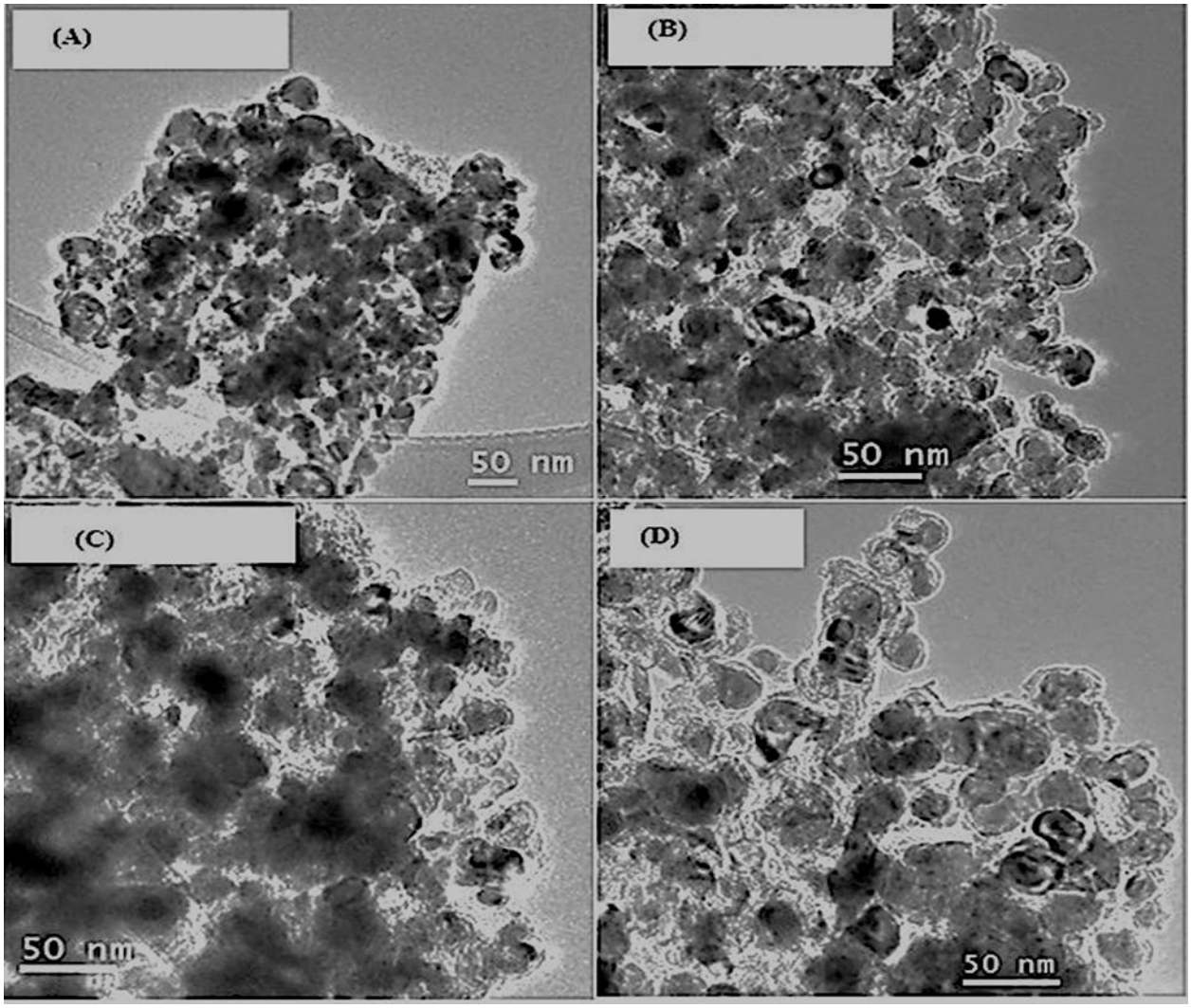

Figure 5(A-D).

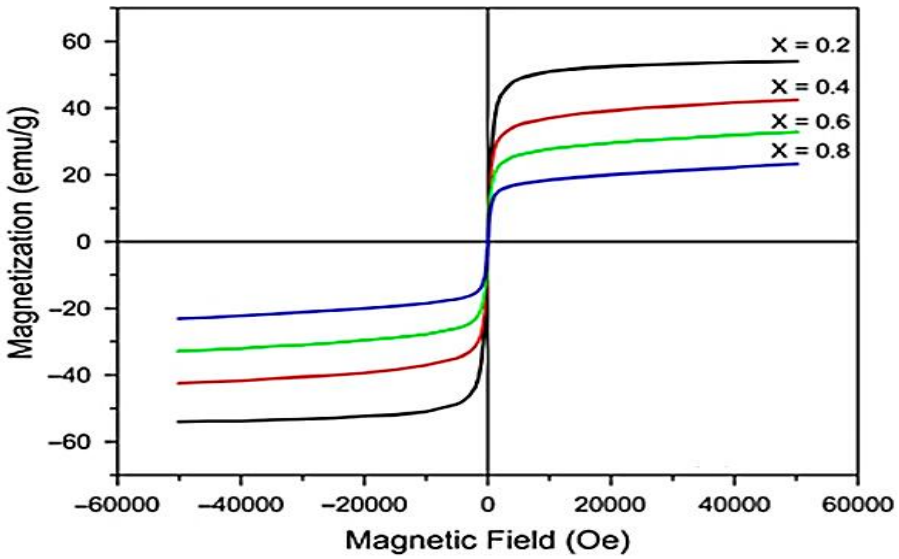

Figure 6.

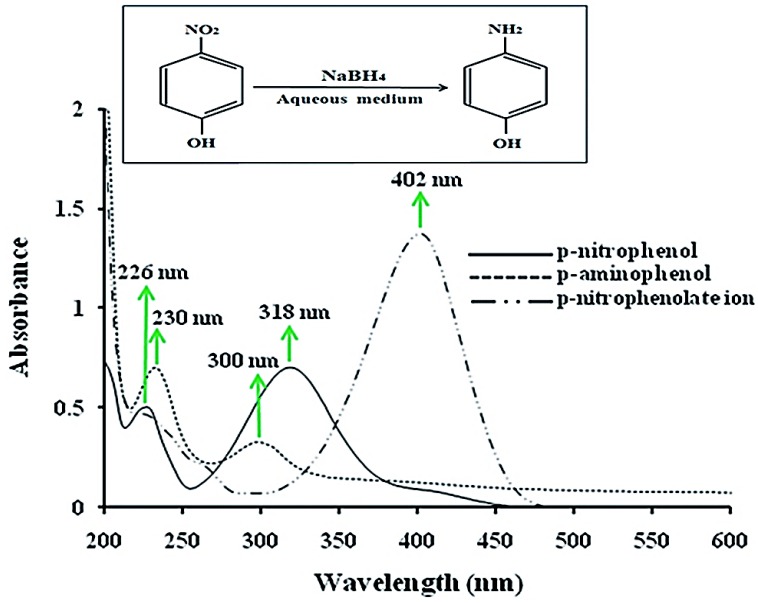

Figure 7.

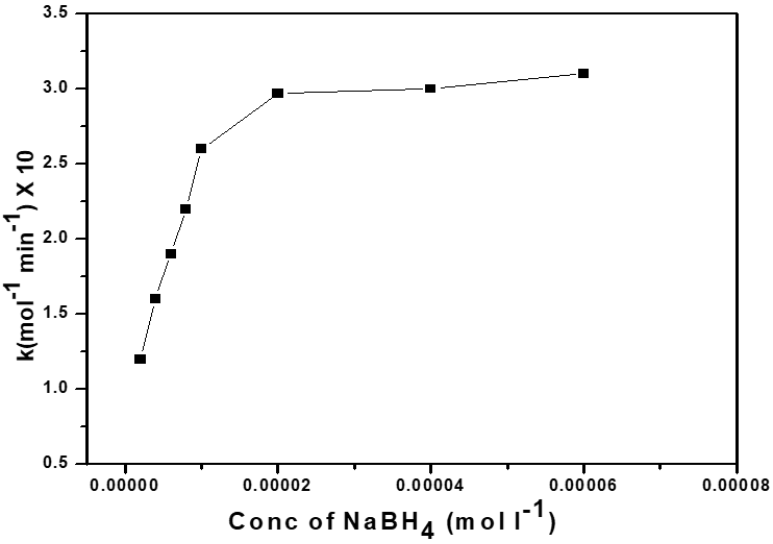

Figure 8.

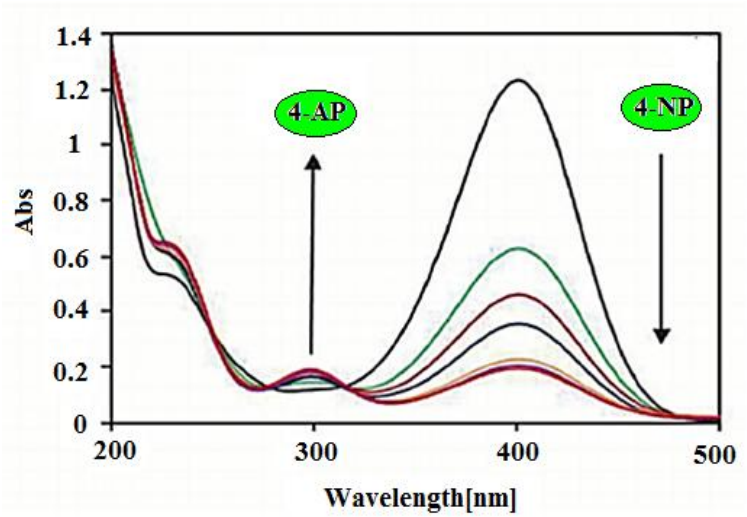

Figure 9.

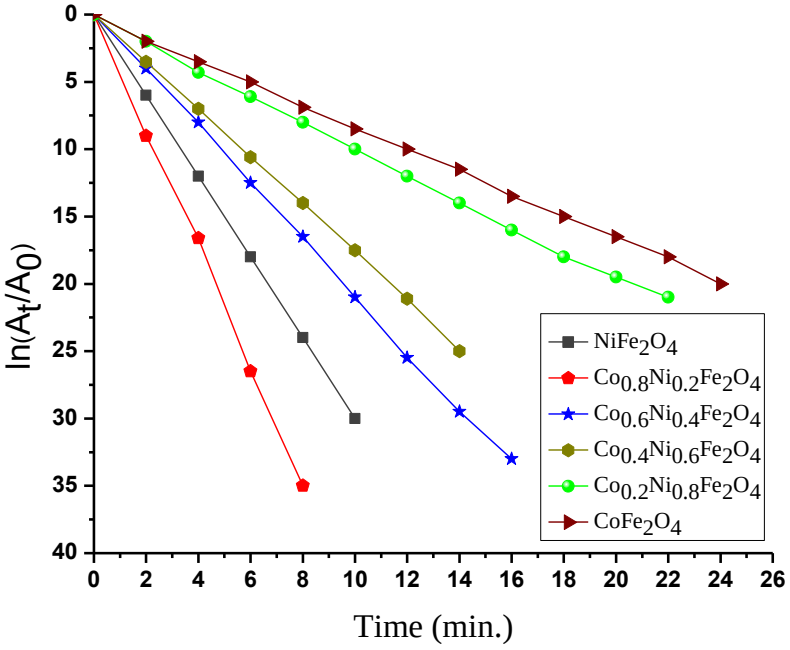
ln(At/A0)
Time (min.)
NiFe2O4
Co0.8Ni0.2Fe2O4
Co0.6Ni0.4Fe2O4
Co0.4Ni0.6Fe2O4
Co0.2Ni0.8Fe2O4
CoFe2O4

Figure 10.